Spatial uniformity of action potentials indicates base-to-apex depolarization and repolarization of rainbow trout (*Oncorhynchus mykiss*) ventricle

Ahmed Badr[1,2,*], Minna Hassinen[1] and Matti Vornanen[1]

[1]University of Eastern Finland, Department of Environmental and Biological Sciences, P.O. Box 111, 80101 Joensuu, Finland

[2]Sohag University, Faculty of Science, Department of Zoology, 82524 Sohag, Egypt

*Address for correspondence: Dr. Ahmed Badr

University of Eastern Finland, Department of Environmental and Biological Sciences

Tel.: +358 41 756 0912

E-mail: ahmed.osman@uef.fi

P.O. Box 111, 80101 Joensuu

Finland

Abstract

The spatial pattern of electrical activation is crucial for a full understanding of fish heart function. However, it remains unclear whether there is regional variation in action potential (AP) morphologies and underlying ion currents. Because the direction of depolarization and spatial differences in the durations of ventricular APs set limits to potential patterns of ventricular repolarization, we determined AP morphologies, underlying ion currents, and ion channel expression in 4 different regions (spongy myocardium; and apex, base, and middle of the compact myocardium), and correlated them with *in vivo* electrocardiogram (ECG) in rainbow trout (*Oncorhynchus mykiss*). ECG recorded from 3 leads indicated that the depolarization and repolarization of AP propagate from base-to-apex, and the main depolarization axis of the ventricle is between +90° and +120°. AP shape was uniform across the whole ventricle, and little regional differences were found in density of repolarizing K^+ currents or depolarizing Ca^{2+} and Na^+ currents and the underlying transcripts of ion channels, providing compelling evidence for the suggested excitation pattern. The spatial uniformity of AP durations and base-to-apex propagation of activation with a relatively slow velocity of propagation indicates no special ventricular conduction pathway in the trout ventricle like the His-Purkinje system of mammalian

Journal of Experimental Biology • Accepted manuscript

hearts. The sequence of repolarization is solely determined by activation time without being affected by regional differences in AP duration.

Key words: Einthoven's triangle, electrical excitation, fish heart, heart axis, ventricular conduction pathway

Introduction

Coordinated contraction of the vertebrate heart is determined by the propagation of action potential (AP) through all cardiomyocytes of the heart. In fish hearts, electrical excitation is initiated in the sinoatrial (SA) pacemaker at the border zone between *sinus venosus* and the atrium (Haverinen and Vornanen, 2007; Jensen, D., 1965; Mackenzie, 1913; Saito, 1969; Saito, 1973; von Skramlik, 1935; Yamauchi and Burnstock, 1968). In the atrial wall, AP propagates quickly along strands of working cardiomyocytes to the atrioventricular (AV) canal, where the velocity of AP propagation slows down, leaving sufficient time to fill the ventricle with blood (Irisawa, 1978; Sedmera et al., 2003). The cycle of electrical excitation of the heart is terminated by a rapidly advancing ventricular AP which triggers ventricular myocytes to contract almost simultaneously. The ventricles of endothermic hearts have a specialized endocardial conducting system that originates from the branches of the His bundles and ramifies as Purkinje fibers among the working ventricular myocytes (Gourdie et al., 1993; Jensen et al., 2012; Sedmera and Gourdie, 2014; Szabóa et al., 1986). Unlike mammalian and avian hearts, histologically specialized conduction path has not been unequivocally demonstrated in fish hearts, although some functional studies suggest the existence of an endocardial conduction pathway in the ventricle of zebrafish (*Danio rerio*) and African lungfish (*Protopterus ethiopicus*) (Arbel et al., 1977; Sedmera et al., 2003).

The rhythmic generation of APs and variable rate of AP propagation through the heart is due to the specialized ion current/channel compositions that produces functionally specific APs for each tissue compartment (Chandler et al., 2009; Greener et al., 2009; Greener et al., 2011; Hassinen et al., 2021; Abramochkin et al., 2022). In general, SA and AV nodes, His bundles and Purkinje fibers, are histologically identifiable from the adjacent working myocardium with characteristic cellular composition, size and structure, arrangement and relative abundance of connective and muscular tissues, or immunohistochemically by specific molecular markers (Anderson et al., 2009; Boyett, 2009; Jensen et al., 2012; Waller et al., 1993a; Waller et al., 1993b). In mammalian and avian ventricles, AP proceeds from the apex-to-base and from endocardium to epicardium, owing to the His-Purkinje system (Autenrieth et al., 1975). The spread of activation in the fish ventricle is still poorly understood, and it is unclear whether there is a specialized ventricular conduction pathway that quickly transmits APs from the AV canal to the apex of the ventricle. Consistent with the putative existence of a ventricular conduction pathway, apex-to-base depolarization of the zebrafish ventricle has been reported (Sedmera et al., 2003; Zhao et al., 2021). However, Jensen et al. (Jensen et al., 2012) reported that

depolarization of the zebrafish ventricle proceeds from base to apex. The reason for the conflicting results is currently unclear. In other studied fish species, including the rainbow trout (*Oncorhynchus mykiss*), the main vector of activation has been reported to go from base to apex (Kibler et al., 2021; Noseda et al., 1962; Vaykshnorayte et al., 2011; Vaykshnorayte et al., 2018).

Because the wave of depolarization (activation) reaches each myocyte at different times, the sequence of ventricular repolarization must be determined by the activation time and the duration of AP at each locus of the ventricular myocardium. Indeed, in mammalian hearts, there are transmural and apicobasal differences in AP duration and underlying ion currents, which affect the repolarization pattern of the ventricles (Bryant et al., 1997; Cheng et al., 1999; Dean and Lab, 1990; McKinnon and Rosati, 2016; Shipsey et al., 1997; Szentadrassy et al., 2005). It is not known, however, whether there is a similar regional variation in AP morphologies and ion channel/current distribution in the fish ventricle. Since the direction of depolarization (i.e., local activation time) and spatial differences in the durations of ventricular APs set limits for possible patterns of ventricular repolarization, we measured cardiac axis (i.e., direction of depolarization) and regional distribution of AP durations to deduce the pattern of ventricular repolarization and the potential presence of a special ventricular conduction pathway in trout ventricle. Based on significant histological differences in the ventricular structure of the fish (compact vs. spongy myocardium), it was hypothesized that there are spatial heterogeneities of electrical activity between the ventricular regions.

Materials and methods

Animals

Adult rainbow trout, both sexes, with the mean (± SEM) body mass of 24.60 ± 1.45 g (n=41) were obtained from the local fish farm (Kontiolahti, Finland). In the animal facilities of the University of Eastern Finland (Joensuu), the fish were reared in 500-liter aquariums with a computer-controlled temperature regulation system (Computec, Joensuu Finland). The temperature of the aquariums was regulated at 12°C and aerated water (O_2 9.7 mg mL^{-1}) flowed through them. The photoperiod was 12:12-h light:dark. The fish were fed 5 times a week (Ewos, Turku, Finland). Experiments were conducted with the permission of the national animal experimental board in Finland (permissions STH252A and ESAVI/8877/2019).

Isolation of ventricular myocytes

The trout were stunned by a blow to the head and killed by pithing. The heart was quickly excised and rinsed in Ca^{2+}-free low Na^{+} solution containing (in mmol L^{-1}): 100 NaCl, 10 KCl, 1.2 KH_2PO_4, 4 $MgSO_4$, 50 taurine, 20 glucose and 10 HEPES [4-(2-hydroxyethyl)-1-piperazineethanesulfonic acid] with pH adjusted to 6.9 at 20°C with KOH. Ventricular myocytes were isolated with enzymatic digestion method described previously in detail (Vornanen, 1997; Vornanen, 1998). First, the heart was perfused for 7-min with Ca^{2+}-free

low-Na^+ saline and then enzymatically digested by a 15-min perfusion with the same solution containing collagenase (Type IA; 0.75 mg ml^{-1}, Sigma, St Louis, MO, USA), trypsin (Type IX; 0.5 mg ml^{-1}, Sigma) and fatty acid-free bovine serum albumin (BSA; 0.75 mg ml^{-1}, Sigma). Both solutions were oxygenated with 100% O_2, and the enzyme solution was recycled using a peristaltic pump. After enzymatic digestion, the ventricle was excised and 4 different regions, 3 parts (apex, middle region, base) from the compact layer and the spongy layer, were carefully separated as schematically indicated in **Figure 1A**. Each part was minced with scissors into small pieces in fresh low-Na solution and dissociated into single myocytes by agitating them through the opening of a Pasteur pipette. Isolated myocytes were stored at 5°C in Ca^{2+}-free low-Na^+ solution and used within 8 h from isolation.

Recording of action potentials (APs)

Ventricular APs were recorded in the current clamp mode of the whole-cell patch-clamp as described earlier (Badr et al., 2017). The compositions of internal (pipette) and external (bath) solutions are show in **Tables 1 and 2**. Patch pipettes were pulled from borosilicate glass (King Precision, Claremont, CA) and when filled with the intracellular saline solution, the mean electrode resistance (means ± SEM) was 2.92 ± 0.07 MΩ (n = 93). The mean capacitive size (means ± SEM) of ventricular myocytes was 31.23 ± 0.80 pF (n = 93). The temperature of the external solution was regulated to 12°C by using a Peltier device (HCC-100A, Dagan, MN, USA). Myocytes were paced at the frequency of 1 Hz. The digitized data were recorded using Clampex 9.2 software (Axon Instruments, Saratoga, CA, USA) and the recordings were analyzed using Clampex 10.4 software package. The following AP parameters were analyzed off-line: resting membrane potential (V_{rest}, mV), threshold potential for AP initiation (TP, mV), critical depolarization (CD = TP − V_{rest}, mV), AP overshoot (OS, mV), AP amplitude (Amp, mV), AP duration 50% repolarization level (APD_{50}, ms), the maximum rate of AP upstroke (+dV dt^{-1}, mV ms^{-1}), and the maximum rate of AP repolarization (−dV dt^{-1}, mV ms^{-1}; **Fig. 1B**).

Recording of ion currents

Ion currents were recorded in the voltage clamp mode of the whole-cell patch-clamp as described earlier in detail (Badr et al., 2017; Badr et al., 2018). Four major ion currents that regulate the shape of ventricular AP in rainbow trout ventricular myocytes were measured: the inward rectifier K^+ current (I_{K1}), the fast component of the delayed rectifier K^+ current (I_{Kr}), L-type Ca^{2+} current (I_{CaL}) and Na^+ current (I_{Na}). The compositions of internal and external solutions used for ion current measurements are shown in **Tables 1 and 2**. When filled patch pipettes with the intracellular saline solution, the mean pipette resistance (means ± SEM) was 3.20 ± 0.04 MΩ (n = 218). The mean capacitive size (means ± SEM) of ventricular myocytes was 38.86 ± 0.69 pF (n = 218). Experimental temperature was 12°C. The size of ion currents is given as current densities (pA pF^{-1}).

Gene expression

Total RNA was extracted from the same regions of the ventricle where myocytes were isolated for patch-clamp recordings (apex, middle part and base of the compact layer and the spongy myocardium, n = 6) by TRI Reagent Solution (Thermo Scientific, Vilnius, Lithuania). Transcript levels were determined in triplicate from each sample using Maxima SYBR Green qPCR Master Mix (Thermo Scientific), specific primers and AriaMx Real-Time PCR System (Agilent Technologies Inc., Santa Clara, CA, USA), as reported previously (Hassinen et al., 2021). The mRNA expression of the studied genes was normalized to the transcript abundance of reference gene DnaJA2 by using ΔCt method (Hassinen et al., 2015).

Recording of electrocardiograms

Electrocardiograms (ECG) were recorded *in vivo* from mildly anesthetized fish (n = 11) in the aquarium room (16℃) as previously described (Badr et al., 2016; Vornanen et al., 2014). ECG recordings were analyzed off-line using LabChart 7.1 software (ADInstruments). Fish were anesthetized with neutralized tricaine methanesulfonate (MS-222; 0.3 mg L^{-1}; Sigma, St Louis, MO, USA) for less than 3 min. When the fish was completely immobile and did not react to handling, it was gently placed on a damp sponge with the abdomen facing up. Aerated water from a 500-L aquarium (O_2 tension about 9 mg L^{-1}) was continuously administered to the gills through an oral tube. To define the electrical axis of the heart (the major direction of the overall electrical activity of the heart in the frontal plane), 3 thin steel electrodes (7-strand Teflon-coated wire, 0.23 mm in diameter; A-M Systems, Carlsborg, WA, USA) were inserted under the ventral skin of the fish to mimic the 3 limb leads of the Einthoven's triangle (**Fig. 4A**). For the lead I (0°), the bipolar electrodes were oriented along the horizontal axis of the heart at the same level (slightly above lower edge of the opercula), with the negative (−) electrode on the right and the positive (+) electrode on the left. For leads II and III, the bipolar electrodes were oriented along the longitudinal axis of the heart. In the lead II (+60°), the negative electrode was positioned at the ventricular base on the right and the positive electrode close to the apex of the heart on the left. In the lead III (+120°), the negative electrode was positioned at the ventricular base on the left and the positive electrode close to the apex of the heart on the right (Dupre et al., 2005). In all leads, the reference electrode was near the anus.

In ECG, a wave of depolarization traveling toward the positive electrode displays a positive voltage on the ECG tracing. Thus, in the case of ventricular depolarization (QRS complex), if the R wave is larger than the S wave, then depolarization propagates towards the positive electrode, but if the S wave is larger than the R wave, then depolarization is propagating away from the positive electrode. If R and S waves are equal in size, then depolarization spreads perpendicular to the vector of that lead (isoelectric). The electrical axis of the fish ventricle can be obtained as a sector overlap in the circle formed by the vectors of the 3 leads. It is noteworthy that if T wave (repolarization of the ventricle) is concordant with QRS complex, i.e., it has the same polarity as QRS wave, then repolarization occurs in opposite direction to depolarization in that lead (Dössel et al.,

2021; Janse et al., 2012). If QRS and T waves are discordant, then repolarization occurs in the same direction as depolarization.

Statistics

The results are represented as means ± SEM. Normality of distribution was tested using Shapiro-Wilk test, and if the data failed the assumption of normality, logarithmic transformations were made. After checking the equality of variances, statistical comparison of mean values of APs, ion currents, mRNA amounts, and ECG parameters were performed using one-way ANOVA. Tukey's and LSD (in the case of equal variances) or Dunnett's T3 (unequal variances) post hoc test was used for paired comparisons. Differences were considered statistically significant when $p<0.05$.

Results

Action potentials

APs were measured in enzymatically isolated ventricular myocytes from 4 different regions (spongy myocardium; and apex, base, and middle region of the compact myocardium) (**Fig. 1A**). APs from spongious myocardium and different regions of the compact ventricular myocardium had similar shapes (**Fig. 1B**). V_{rest}, TP, CD, OS, $-dV\ dt^{-1}$ and APD_{50} were not different between the different regions ($p>0.05$) (**Fig. 1C-E**). Amplitude of the AP was 5.8% higher in spongiosa compared to apex ($p<0.05$), and the maximum rate of depolarization ($+dV\ dt^{-1}$) was slightly higher (22.3-23.7%) in middle region and spongiosa than base and apex (**Fig. 1F;** $p<0.05$).

Outward K^+ currents and transcript expression of K^+ channels

I_{K1} current was elicited from the holding potential of –80 mV by voltage ramps from +60 to −120 mV at the frequency of 0.2 Hz using the established voltage protocol (**Fig. 2A**). There were no differences in I_{K1} density between different regions of the ventricle either for the inward current (I.C.) or the outward current (O.C.) (**Fig. 2B**). The I_{K1} current is produced by various Kir2 channels, of which Kir2.4, Kir2.2b and Kir2.1a account for approximately 98% of the I_{K1} in rainbow trout ventricular myocytes (Hassinen et al., 2021). Consistent with the I_{K1} density, there were no differences in the expression of the 3 major isoforms of I_{K1}-producing Kir2 genes between the different regions of the ventricle (**Fig. 2C**).

I_{Kr} current was elicited from the holding potential of –80 mV by 2-steps voltage protocol at the frequency of 0.2 Hz using the established voltage protocol (**Fig. 2D**). There were no significant differences in I_{Kr} density between different regions of the ventricle (**Fig. 2E**). The I_{Kr} current is produced by various erg genes, of which KCNH6a (erg2) alone accounts for approximately 99.7% of the current in rainbow trout ventricle (Hassinen et al., 2021). Consistent with the I_{Kr} density, there were no differences in the expression of the two isoforms of I_{Kr}-producing erg genes (KCNH6a and KCNH2bb) between the different regions of the ventricle (**Fig. 2F**).

Inward currents and transcript expression of Ca^{2+} and Na^{+} channels

Ca^{2+} current (I_{Ca}) was elicited from the holding potential of −80 mV in the presence 0.5 µM TTX which completely blocks I_{Na} (**Fig. 3A**). The threshold voltage of I_{Ca} was about −30 mV and the peak density of I_{Ca} occurred at 0 mV for all 4 regions of the trout ventricle suggesting that major part of the charge was carried by L-type Ca^{2+} current (I_{CaL}). There were no statistically significant differences in the peak I_{Ca} density at 0 mV between different regions of the ventricle (**Fig. 3B**). I_{Ca} of trout ventricle is produced by a variety of Ca^{2+} channel genes (Hassinen et al., 2021). L-type Ca^{2+} channel cacna1c was the major component in all regions except the base, where cacna1c and the T-type Ca^{2+} channel cacna1ga were equally expressed (**Fig. 3C**). Of the minor Ca^{2+} components, L-type Ca^{2+} channel cacna1daa and T-type Ca^{2+} channel cacna1ha were more highly expressed in the base than in other regions of the ventricle (p<0.05), while no differences were in T-type Ca^{2+} channel cacna1hb between different regions of the ventricle. The combined expression level of all Ca^{2+} channels did not differ between the four tissue regions (p>0.05; **Fig. 3C**).

Na^{+} current (I_{Na}) was elicited from the holding potential of −120 mV every 1 s (**Fig. 3D**). The peak current density was between −30 and −20 mV. There were no statistically significant differences in the peak current density of I_{Na} between different regions of the ventricle (**Fig. 3E**). I_{Na} is produced by several Na^{+} channel alpha subunits in the rainbow trout ventricle, of which SCN4Aba and SCN5LAbb are the dominant isoforms (Hassinen et al., 2021). Consistent with the I_{Na} density, there were no statistically significant differences in the combined expression of the 4 alpha subunit isoforms between different regions of the ventricle (p>0.05) (**Fig. 3F**). However, the expression of SCN4Abb was higher in the base than in other regions, and the expression of SCN5LAba in the base was lower than that in the apex and spongiosa.

Determination of heart axis

The positions of the bipolar electrodes and the vectors of 3 ECG leads, and typical recordings from leads I, II and III are shown in **Figure 4A, B**. P wave and QRS complex correspond atrial and ventricular depolarization, respectively, whereas the T wave represents the repolarization of the ventricle. R wave is bigger than S wave (positive QRS polarity) in leads II (+60°) and III (+120°) but smaller than S wave (negative QRS polarity) in lead I (0°) (**Fig. 4B, C**). Furthermore, the amplitude of the R wave is about 50% higher in lead III than leads I and II (p<0.05; **Fig. 4E**) suggesting that the vector of the lead III is closest to the heart axis. Indeed, the overlap of the lead vectors (shaded areas of circles in **Fig. 4F**) indicate that the cardiac axis is between +90° and +120°, i.e., the main axis of ventricular depolarization is from base to apex. T wave is discordant with R wave in the 3 leads suggesting that repolarization and depolarization of the ventricle in these leads occur in the same direction (**Fig. 4B-D**). Given that the lead III is almost parallel to the heart axis, the discordant T wave indicates that the main direction of repolarization in trout ventricle is from base to apex.

Mean duration (± SEM) of the QRS complex (activation), measured from the 3 EGC leads was 51.5±1.2 ms. Since the total length of the trout ventricle was about 6 mm, the rate of AP propagation in the ventricular wall was approximately 0.12 m s^{-1}.

Discussion

Analysis of APs, ion currents, and transcript expression of ion channel α-subunits show little regional heterogeneity in molecular and cellular basis of electrical excitation in the rainbow trout ventricle. Measurement of APs and ion currents indicate that electrical excitation is homogenous at the level of isolated ventricular myocytes. This differs from several observations on mammalian cardiac myocytes, which show large regional differences in the shape of ventricular AP, underlying ion currents and ion channel expression (Antelevitch and Fish, 2001; Gaborit et al., 2007; McKinnon and Rosati, 2016; Schram et al., 2002; Szentadrassy et al., 2005; Watanabe et al., 1983). It might be assumed that the situation would be different if APs were measured from an intact fish ventricle. In multicellular tissue, myocytes are electrically coupled to each other, and electrotonic current flow between myocytes will attenuate, not increase, differences in AP shape (Anyukhovsky et al., 1999; Janse et al., 2012).

The conduction of depolarization and repolarization of the endothermic (mammalian and avian) hearts can be reduced to the consensus view that the major direction of depolarization is from apex to base and that the last activated regions repolarize first because they have the shortest APs. Therefore, the main direction of repolarization is from base to apex and from epicardium to endocardium, although this concept is questioned (Christian and Scher, 1967; Opthof et al., 2017). This excitation pattern is structurally and functionally based on the rapid conduction pathway of the His-Purkinje system and apicobasal and transmural differences of AP durations and ion current densities. Due to the fast conducting His-Purkinje system, the effect of activation time to repolarization pattern may be small in endothermic hearts (Ramanathan et al., 2006). On the other hand, hearts of embryonic endotherms and adult ectotherms seem to lack an anatomically distinct ventricular conduction pathway similar to the His-Purkinje system, and therefore in these hearts activation may occur from base to apex (Jensen et al., 2012). The present ECG recordings indicate that the main cardiac axis is indeed oriented craniocaudally, suggesting that depolarization of the trout ventricle occurs from base to apex. This is consistent with activation patterns of cod (*Gadus morhua*), pike (*Esox Lucius*) and rainbow trout ventricle determined by multielectrode arrays (Azarov et al., 2013; Kibler et al., 2021; Vaykshnorayte et al., 2011; Vaykshnorayte et al., 2022). In these teleost species, the earliest activation occurs in the endocardial surface of the dorsal base near the atrioventricular orifice and spreads from there toward the ventral areas of the base and at the same time to the apex of the ventricle. Optical mapping of activation in the zebrafish heart indicates a similar activation pattern to that of cod, pike and trout (Jensen et al., 2012). However, the results for zebrafish are partly contradictory, as activation has also been shown to propagate from

apex to base (Sedmera et al., 2003; Zhao et al., 2021). Two of the zebrafish studies (Jensen et al., 2012; Zhao et al., 2021) used the same voltage-sensitive dye, di-4-ANEPPS, for optical mapping. The fact that a different conclusion was reached using the same recording method suggests that differences in experimental conditions might explain the conflicting results. Since the depolarization pattern has only been studied in a few teleost species, it is impossible to make any generalization of the ventricular activation pattern in fish. However, current observations indicate base-to-apex type of activation in most of the species studied.

The direction of ventricular repolarization is dependent on the spatial spread of depolarization (activation time) and AP duration (Janse et al., 2012). The current ECG recordings in rainbow reveal that the repolarization proceeds from base to apex. In the 3 leads, T wave had an opposite polarity than R wave indicating that repolarization proceeded in the same direction as depolarization in these leads. The base-to-apex repolarization is consistent with multielectrode array studies in this species which showed earliest repolarization in the ventral base and then in dorsal base and apex of the ventricle (Kibler et al., 2021). The homogeneity of AP durations throughout the trout ventricle is consistent with the base-to-apex repolarization pattern. In fact, similarity of AP durations does not allow for apex-to-base repolarization. In rainbow trout ventricle, activation reaches the apex within about 52 ms from the first depolarization at the base. During this time, APs of the basal myocytes have already started repolarization, which therefore must proceed towards the apex in the same order as depolarization due to the spatial similarity of AP durations. The spatial homogeneity of AP durations is supported by similar density of the main depolarizing and repolarizing ion currents and similar transcript levels of ion channel α-subunits in different parts of the ventricle. Consistent with this, the ventricle of summer-acclimatized rainbow trout at 18℃ shows little differences in activation time and activation-repolarization interval (Vaykshnorayte et al., 2022). Also consistent with the current AP duration data, multielectrode array studies have shown that repolarization time is similar at the base and apex of the trout ventricle at the sinus rate (Kibler et al., 2021). Notably, when the combined data from the 3 regions of the compact myocardium were compared with that of the spongy layer, practically no differences were found in APs, ion currents and ion channel expression (**Supplementary figure 1S**). This strongly suggests the absence of transmural heterogeneity of activation and repolarization in the trout ventricle. However, Vaykshnorayte et al. (2022) found transmural and apicobasal differences in activation time and activation-repolarization interval in the ventricle of winter-acclimated rainbow trout at 3℃, suggesting that the patterns of activation and repolarization may be temperature-dependent. Repolarization pattern of ventricular epicardium of the pike heart is shown to occur mainly in apex-to-base direction, although an additional area of early repolarization was found at the posterior ventricular base, i.e., at the site of early depolarization (Vaykshnorayte et al., 2011). Apex-to-base repolarization requires that the durations of AP become shorter from the base of the ventricle towards the apex of the ventricle. Consistent with this, the repolarization time of the apex is slightly shorter in the apex than base of the pike ventricle (Vaykshnorayte et al., 2011). Similar difference in

repolarization as between trout and pike is found also between canine and human hearts: in human ventricles, activation and repolarization proceed in opposite directions, whereas the activation and repolarization follow the same pattern in dog ventricles. Accordingly, in the human QRS and T waves are concordant but in the dog, they are discordant (Janse et al., 2012). It seems that the repolarization of the vertebrate ventricle(s) is more variable than depolarization, both within and between species (Opthof et al., 2017). The functional significance of different repolarization patterns remains to be elucidated.

Mammalian ventricles have two types of cardiac myocytes: working ventricular myocytes and conducting Purkinje fibers, the former showing region specific characteristics of excitability (epi- midmyo- and endocardial myocytes) (Anyukhovsky et al., 1999). In contrast to mammalian ventricles, the trout ventricle seems to have only working myocardial cells which are electrophysiologically homogenous through the ventricular myocardium. This may suggest that specific conduction fibers are absent and therefore electrical excitation propagates along the working myocardial cells throughout the ventricle, which may be an evolutionally old feature and common to the hearts of all ectotherms (Jensen et al., 2012; Boukens et al, 2019). In trout ventricle at 16℃, the rate of AP propagation was about 0.12 m s^{-1}. In mammalian Purkinje fibers the rate of AP propagation at 37℃ is 2 m s^{-1} or slightly higher (Cranefield et al., 1971; Dominguez and Fozzard, 1970), whereas in working ventricular muscle it is about 0.6 m s^{-1} (Kelly et al., 2013; McIntyre and Fry, 1997). Using Q_{10}-value of 2.0, the rate of AP propagation in mammalian Purkinje fibers would be about 0.47 m s^{-1} and 0.14 m s^{-1} in working ventricular myocardium at 16℃. The fact that the rate of AP propagation in the trout ventricle is only about 1/4 of the rate of mammalian Purkinje fibers, but similar to the rate of mammalian working myocardium suggests that conduction does not involve Purkinje fiber-type myocytes. However, if present, the conducting fibers should be electrophysiologically clearly recognizable (e.g. by large I_{Na} and fast +dV dt^{-1}) from the working cardiac myocytes (Dangman et al., 1982; Makielski et al., 1987). The current study includes patch-clamp recordings from over 300 myocytes from different regions, which is only a tiny fraction of the total myocyte population of the ventricle, and therefore it is possible not a single conducting fiber was recorded. When searching for a specialized ventricular conducting system, it should be histologically discrete and insulated by a sheath of fibrous tissue from the adjacent working myocardium (Anderson et al., 2009) and characterized by a high density of molecular markers of a fast-conducting tract (e.g. connexins, sodium channels) (Haufe et al., 2005; Kanter et al., 1993). Indeed, Boukens et al. (2019) hypothesized that the electrical conduction delay in the ventricle of ectotherms compared to mammals might be due to the tortuous structure of the spongious myocardium, whereas the compact architecture of mammalian ventricles accelerates electrical conduction independently of the conduction system, as occurs in the mammalian atria.

To our knowledge, this is the first study to look at the expression of AP waveforms, ion currents, and ion channels in the fish ventricle. Findings at all organization levels (APs, ion currents, ion channel expression) indicate regional homogeneity of electrical excitation throughout the trout ventricle. At the organismal level, these findings are consistent with

the base-to-apex spread of both depolarization and repolarization, which does not require a specialized ventricular conduction system. From the perspective of ventricular function, this means that at the onset of contraction, the pressure is directed toward the apex of the ventricle, forcing blood to flow through the network of spongious myocardium. Because the basal area relaxes first, blood flows from the apical ventricle towards the base and into the *bulbus arteriosus* is facilitated by the early increase in the volume of the basal ventricle. Future studies should investigate whether the absence of specialized ventricular conduction system, characterized by high I_{Na} density and fast AP upstroke velocity, sets the upper limit to the heart rate of fish at critically high temperatures (Vornanen, 2020) .

Acknowledgements

We thank Anita Kervinen for taking care of fishes and preparing solutions for the patch-clamp experiments. The present study was supported by the Academy of Finland (project 15051 to M. Vornanen).

Conflict of interest

The authors declare that they have no known competing financial or personal interests that could influence the present study.

References

Abramochkin, D.V., Filatova, T.S., Pustovit, K.B., Voronina, Y.A., Kuzmin, V.S. and Vornanen, M. (2022). Ionic currents underlying different patterns of electrical activity in working cardiac myocytes of mammals and non-mammalian vertebrates. *Comp. Biochem. Physiol. Part A* **268**, 111204.

Anderson, R. H., Yanni, J., Boyett, M. R., Chandler, N. J. and Dobrzynski, H. (2009). The anatomy of the cardiac conduction system. *Clin. Anat.* **22,** 99-113.

Antelevitch, C. and Fish, J. (2001). Electrical heterogeneity within the ventricular wall. *Basic Res. Cardiol.* **96,** 517-527.

Anyukhovsky, E. P., Sosunov, E. A., Gainullin, R. Z. and Rosen, M. R. (1999). The controversial M cell. *J. Cardiovasc. Electrophysiol.* **10,** 244-260.

Arbel, E. R., Liberthson, R., Langendorf, R., Pick, A., Lev, M. and Fishman, A. P. (1977). Electrophysiological and anatomical observations on the heart of the African lungfish. *Am. J. Physiol.* **232,** H24-H34.

Autenrieth, G., Surawicz, B. and Kuo, C. S. (1975). Sequence of repolarization on the ventricular surface in the dog. *Am. Heart J.* **89,** 463-469.

Azarov, J. E., Kibler, N. A., Vaykshnorayte, M. A., Tsvetkova, A. S., Kharin, S. N., Vityazev, V. A. and Shmakov, D. N. (2013). Effect of heart electric stimulation on repolarization of ventricular myocardium of fish and amphibians. *J. Evol. Biochem. Physiol.* **49,** 165-174.

Badr, A., El-Sayed, M. F. and Vornanen, M. (2016). Effects of seasonal acclimatization on temperature-dependence of cardiac excitability in the roach, *Rutilus rutilus*. *J. Exp. Biol.* **219,** 1495-1504.

Badr, A., Hassinen, M., El-Sayed, M. F. and Vornanen, M. (2017). Effects of seasonal acclimatization on action potentials and sarcolemmal K^+ currents in roach (*Rutilus rutilus*) cardiac myocytes. *Comp. Biochem. Physiol. A* **205,** 15-27.

Badr, A., Korajoki, H., Abu-Amra, E., El-Sayed, M. F. and Vornanen, M. (2018). Effects of seasonal acclimatization on thermal tolerance of inward currents in roach (Rutilus rutilus) cardiac myocytes. *J. Comp. Physiol. B* **188,** 255-269.

Boukens, B.J., Kristensen, D.L., Filogonio, R., Carreira, L.B., Sartori, M.R., Abe, A.S., Currie, S., Joyce, W., Conner, J., Opthof, T., Crossley II, D.A., Wang, T. and Jensen, B. (2019). The electrocardiogram of vertebrates: Evolutionary changes from ectothermy to endothermy. *Prog. Biophys. Mol. Biol.* **144**, 16-29.

Boyett, M. R. (2009). 'And the beat goes on 'The cardiac conduction system: the wiring system of the heart. *Exp. Physiol.* **94,** 1035-1049.

Bryant, S. M., Shipsey, S. J. and Hart, G. (1997). Regional differences in electrical and mechanical properties of myocytes from guinea-pig hearts with mild left ventricular hypertrophy. *Cardiovasc. Res.* **35,** 315-323.

Chandler, N. J., Greener, I. D., Tellez, J. O., Inada, S., Musa, H., Molenaar, P., Difrancesco, D., Baruscotti, M., Longhi, R., Anderson, R. H. et al. (2009). Molecular architecture of the human sinus node: insights into the function of the cardiac pacemaker. *Circulation* **119,** 1562-1575.

Cheng, J., Kamiya, K., Liu, W., Tsuji, Y., Toyama, j. and Kodama, I. (1999). Heterogeneous distribution of the two components of delayed rectifier K current: a potential mechanism of the proarrhythmic effects of methanesulfonanilideclass III agents. *Cardiovasc. Res.* **43,** 135-147.

Christian, E. and Scher, A. M. (1967). The effect of ventricular depolarization on the sequence of ventricular repolarization. *Am. Heart J.* **74,** 530-535.

Cranefield, P. F., Klein, H. O. and Hoffman, B. F. (1971). Conduction of the cardiac impulse: I. Delay, block, and one-way block in depressed Purkinje fibers. *Circ. Res.* **28,** 199-219.

Dangman, K. H., Danilo Jr, P., Hordof, A. J., Mary-Rabine, L., Reder, R. F. and Rosen, M. R. (1982). Electrophysiologic characteristics of human ventricular and Purkinje fibers. *Circulation* **65,** 362-368.

Dean, J. W. and Lab, M. J. (1990). Regional changes in ventricular excitability during load manipulation of the in situ pig heart. *J. Physiol.* **429,** 387-400.

Dominguez, G. and Fozzard, H. A. (1970). Influence of extracellular K concentration on cable properties and excitability of sheep cardiac Purkinje fibers. *Circ. Res.* **26,** 565-574.

Dössel, O., Luongo, G., Nagel, C. and Loewe, A. (2021). Computer modeling of the heart for ECG interpretation—a review. *Hearts* **2,** 350-368.

Dupre, A., Vincent, S. and Iaizzo, P. A. (2005). Basic ECG theory, recordings, and interpretation. In *Handbook of cardiac anatomy, physiology, and devices* (ed. P. A. Iaizzo), pp. 191-201: Springer.

Gaborit, N., Le Bouter, S., Szuts, V., Varro, A., Escande, D., Nattel, S. and Demolombe, S. (2007). Regional and tissue specific transcript signatures of ion channel genes in the non-diseased human heart. *J. Physiol.* **582,** 675-693.

Gourdie, R. G., Green, C. R., Severs, N. J., Anderson, R. H. and Thompson, R. P. (1993). Evidence for a distinct gap-junctional phenotype in ventricular conduction tissues of the developing and mature avian heart. *Circ. Res.* **72,** 278-289.

Greener, I. D., Monfredi, O., Inada, S., Chandler, N. J., Tellez, J. O., Atkinson, A., Taube, M. A., Billeter, R., Anderson, R. H., Efimov, I. R. et al. (2011). Molecular architecture of the human specialised atrioventricular conduction axis. *J. Mol. Cell. Cardiol.* **50,** 642-651.

Greener, I. D., Tellez, J. O., Dobrzynski, H., Yamamoto, M., Graham, G. M., Billeter, R. and Boyett, M. R. (2009). Ion channel transcript expression at the rabbit atrioventricular conduction axis. *Circ. Arrhythm. Electrophysiol.* **2,** 305-315.

Hassinen, M., Dzumaniiazova, I., Abramochkin, D. V. and Vornanen, M. (2021). Ionic basis of atrioventricular conduction: ion channel expression and sarcolemmal ion currents of the atrioventricular canal of the rainbow trout (Oncorhynchus mykiss) heart. *J. Comp. Physiol. B* **191,** 327-346.

Hassinen, M., Haverinen, J., Hardy, M. E., Shiels, H. A. and Vornanen, M. (2015). Inward rectifier potassium current (I_{K1}) and Kir2 composition of the zebrafish (*Danio rerio*) heart. *Pflüg. Arch.* **467,** 2437-2446.

Haufe, V., Cordeiro, J. M., Zimmer, T., Wu, Y. S., Schiccitano, S., Benndorf, K. and Dumaine, R. (2005). Contribution of neuronal sodium channels to the cardiac fast sodium current INa is greater in dog heart Purkinje fibers than in ventricles. *Cardiovasc. Res.* **65,** 117-127.

Haverinen, J. and Vornanen, M. (2007). Temperature acclimation modifies sinoatrial pacemaker mechanism of the rainbow trout heart. *Am. J. Physiol.* **292,** R1023-R1032.

Irisawa, H. (1978). Comparative physiology of the cardiac pacemaker mechanism. *Physiol. Rev.* **58,** 461-498.

Janse, M. J., Coronel, R., Opthof, T., Sosunov, E. A., Anyukhovsky, E. P. and Rosen, M. R. (2012). Repolarization gradients in the intact heart: transmural or apico-basal? *Prog. Biophys. Mol. Biol.* **109,** 6-15.

Jensen, B., Boukens, B. J. D., Postma, A. V., Gunst, Q. D., van den Hoff, M. J., Moorman, A. F. M., Wang, T. and Christoffels, V. M. (2012). Identifying the evolutionary building blocks of the cardiac conduction system. *PLoS One* **7,** e44231.

Jensen, D. (1965). The aneural heart of the hagfish. *Ann. NY Acad. Sci.* **127,** 443-458.

Kanter, H. L., Laing, J. G., Beau, S. L., Beyer, E. C. and Saffitz, J. E. (1993). Distinct patterns of connexin expression in canine Purkinje fibers and ventricular muscle. *Circ. Res.* **72,** 1124-1131.

Kelly, A., Ghouri, I. A., Kemi, O. J., Bishop, M. J., Bernus, O., Fenton, F. H., Myles, R. C., Burton, F. L. and Smith, G. L. (2013). Subepicardial action potential characteristics are a function of depth and activation sequence in isolated rabbit hearts. *Circ. Arrhythm. Electrophysiol.* **6,** 809-817.

Kibler, N. A., Nuzhny, V. P., Kharin, S. N. and Shmakov, D. N. (2021). Effect of atrial artificial electrical stimulation on depolarization and repolarization and hemodynamics of the heart ventricle in rainbow trout Oncorhynchus mykiss. *Fish Physiol. Biochem.* **47,** 1329-1339.

Mackenzie, I. (1913). The excitatory and connecting muscular system of the heart. *Trans. Int. Cong. Med. Lond.* **Sect. III,** 121-150.

Makielski, J. C., Sheets, M. F., Hanck, D. A., January, C. T. and Fozzard, H. A. (1987). Sodium current in voltage clamped internally perfused canine cardiac Purkinje cells. *Biophys. J.* **52,** 1-11.

McIntyre, H. and Fry, C. H. (1997). Abnormal action potential conduction in isolated human hypertrophied left ventricular myocardium. *J. Cardiovasc. Electrophysiol.* **8,** 887-894.

McKinnon, D. and Rosati, B. (2016). Transmural gradients in ion channel and auxiliary subunit expression. *Prog. Biophys. Mol. Biol.* **122,** 165-186.

Noseda, V., Chiesa, F. and Marchetti, R. (1962). Intracardiac electrocardiography in fishes. *Experienta* **18,** 380-381.

Opthof, T., Remme, C. A., Jorge, E., Noriega, F., Wiegerinck, R. F., Tasiam, A., Beekman, L., Alvarez-Garcia, J., Munoz-Guijosa, C. and Coronel, R. (2017). Cardiac activation–repolarization patterns and ion channel expression mapping in intact isolated normal human hearts. *Heart Rhythm* **14,** 265-272.

Ramanathan, C., Jia, P., Ghanem, J., Ryu, K. and Rudy, Y. (2006). Activation and repolarization of the normal human heart under complete physiological conditions. *PNAS* **103,** 6309-6314.

Saito, T. (1969). Electrophysiological studies on the pacemaker of several fish hearts. *Zool. Mag.* **78,** 291-296.

Saito, T. (1973). Effects of vagal stimulation on the pacemaker action potentials of carp heart. *Comp. Biochem. Physiol. A* **44A,** 191-199.

Schram, G., Pourrier, M., Melnyk, P. and Nattel, S. (2002). Differential distribution of cardiac ion channel Expression as a basis for regional specialization in electrical function. *Circ. Res.* **90,** 939-950.

Sedmera, D. and Gourdie, R. G. (2014). Why do we have Purkinje fibers deep in our heart? *Physiol. Res.* **63 (Suppl. 1),** S9-S18.

Sedmera, D., Reckova, M., deAlmeida, A., Sedmerova, M., Biermann, M., Volejnik, J., Sarre, A., Raddatz, E., McCarthy, R. A., Gourdie, R. G. et al. (2003). Functional and morphological evidence for a ventricular conduction system in zebrafish and *Xenopus* hearts. *Am. J. Physiol.* **284,** H1152-H1160.

Shipsey, S. J., Bryant, S. M. and Hart, G. (1997). Effects of hypertrophy on regional action potential characteristics in the rat left ventricle: a cellular basis for T-wave inversion? *Circulation* **96,** 2061-2068.

Szabóa, E., Virágh, S. and Challice, C. E. (1986). The structure of the atrioventricular conducting system in the avian heart. *Anat. Rec.* **215,** 1-9.

Szentadrassy, N., Banyasz, T., Biro, T., Szabo, G. y., Toth, B. I., Magyar, J., Lazar, J., Varro, A., Kovacs, L. and Nanasi, P. P. (2005). Apico–basal inhomogeneity in distribution of ion channels in canine and human ventricular myocardium. *Cardiovasc. Res.* **65,** 851-860.

Vaykshnorayte, M. A., Azarov, J. E., Tsvetkova, A. S., Vityazev, V. A., Ovechkin, A. O. and Shmakov, D. N. (2011). The contribution of ventricular apicobasal and transmural repolarization patterns to the development of the T wave body surface potentials in frogs (*Rana temporaria*) and pike (*Esox lucius*). *Comp. Biochem. Physiol. A* **159,** 39-45.

Vaykshnorayte, M. A., Vityazev, V. A. and Azarov, J. E. (2022). Seasonal changes of electrophysiological heterogeneities in the rainbow trout ventricular myocardium. *Curr. Res. Physiol.* **00,** 000-000.

Vaykshnorayte, M. A., Vityazev, V. A. and Azarov, Y. E. (2018). The sequence of activation of the ventricular myocardium of the Atlantic cod (Gadus morhua marisalbi). *Proc. Komi Sci. Cent.* **4,** 431-435.

von Skramlik, E. (1935). Über den Kreislauf bei den Fischen. *Ergeb. Biol.* **11,** 1-130.

Vornanen, M. (1997). Sarcolemmal Ca influx through L-type Ca channels in ventricular myocytes of a teleost fish. *Am. J. Physiol.* **272,** R1432-R1440.

Vornanen, M. (1998). L-type Ca current in fish cardiac myocytes: effects of thermal acclimation and β-adrenergic stimulation. *J. Exp. Biol.* **201,** 533-547.

Vornanen, M. (2020). Feeling the heat: source-sink mismatch as a mechanism underlying the failure of thermal tolerance. *J. Exp. Biol.* **223.16,**.

Vornanen, M., Haverinen, J. and Egginton, S. (2014). Acute heat tolerance of cardiac excitation in the brown trout (*Salmo trutta fario*). *J. Exp. Biol.* **217,** 299-309.

Waller, B. F., Gering, L. E., Branyas, N. A. and Slack, J. D. (1993a). Anatomy, histology, and pathology of the cardiac conduction system: Part I. *Clin. Cardiol.* **16,** 249-252.

Waller, B. F., Gering, L. E., Branyas, N. A. and Slack, J. D. (1993b). Anatomy, histology, and pathology of the cardiac conduction system: Part II. *Clin. Cardiol.* **16,** 347-352.

Watanabe, T., Delbridge, L. M., Bustamante, O. J. and McDonald, T. F. (1983). Heterogeneity of the action potential in isolated rat ventricular myocytes and tissue. *Circ. Res.* **52,** 280-290.

Yamauchi, A. and Burnstock, G. (1968). An electronmicroscopic study on the innervation of the trout heart. *J. Comp. Neurol.* **132,** 567-588.

Zhao, Y., James, N. A., Beshay, A. R., Chang, E. E., Lin, A., Bashar, F., Nguyen, B. and Nguyen, T. P. (2021). Adult zebrafish ventricular electrical gradients as tissue mechanisms of ECG patterns under baseline vs. oxidative stress. *Cardiovasc. Res.* **117,** 1891-1907.

Figures and Tables

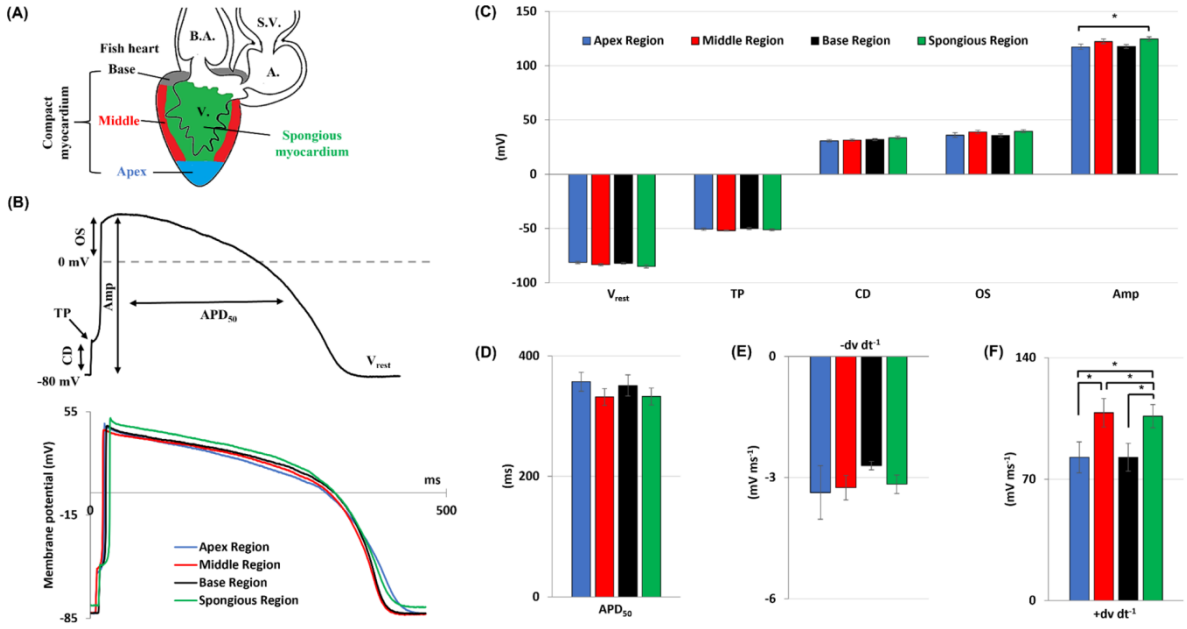

Fig. 1. Ventricular action potentials (APs) waveforms of rainbow trout heart at different regions of the ventricular myocardium (spongy myocardium; and apex, base, and middle regions of the compact myocardium) at 12°C. (**A**) Schematic presentation of myocytes sampling from different locations of the trout ventricle. (**B**) Identification of different measured AP parameters (**top**), and representative registrations of APs from 4 different ventricular regions (**bottom**). (**C**) Mean values of resting membrane potential (V_{rest}), threshold potential for AP initiation (TP), critical depolarization (CD), AP overshoot (OS), and AP amplitude (Amp) for the 4 different ventricular regions. (**D-F**) Mean values of action potential duration at 50% level of repolarization (APD_{50}) (**D**), maximum rate of repolarization ($-dV\ dt^{-1}$) (**E**), and depolarization ($+dV\ dt^{-1}$) (**F**). The results are means (± SEM) of 23-24 myocytes from 10 fishes. An asterisk (*) indicates statistically significant differences ($p < 0.05$; one-way ANOVA) between mean values. B.A., bulbus arteriosus; S.V., sinus venosus; A., atrium; V., ventricle.

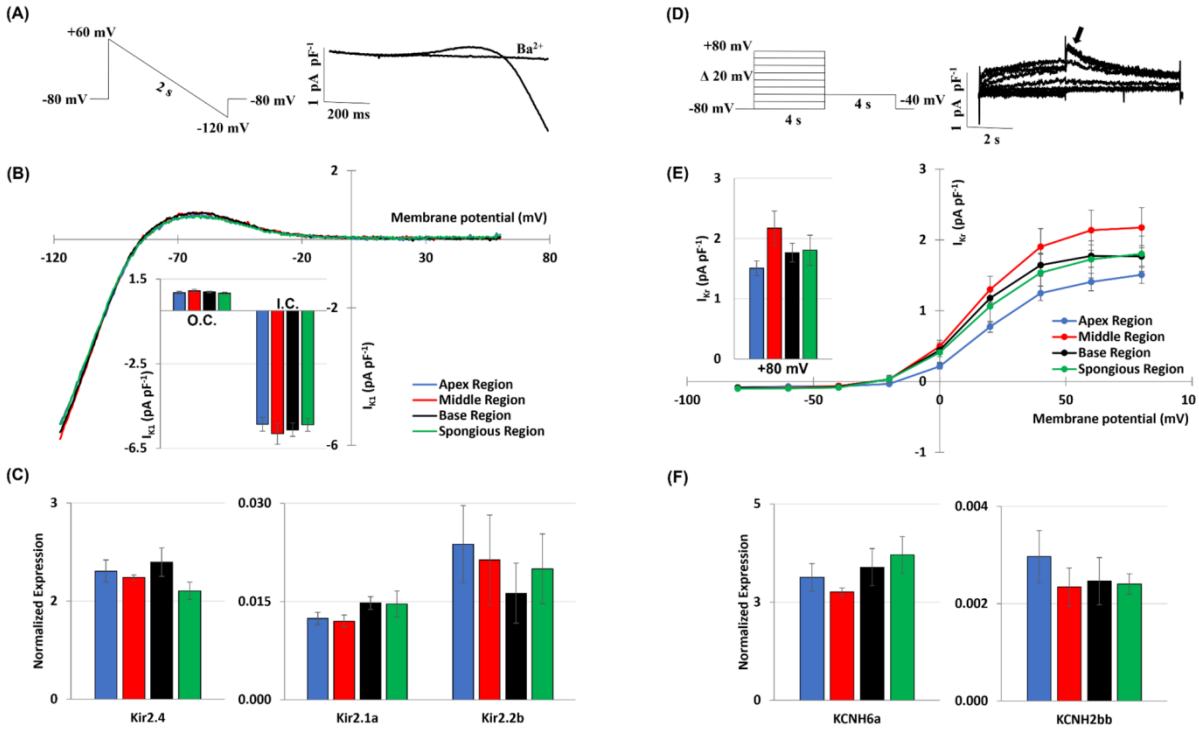

Fig. 2. Inward and delayed rectifier K^+ currents in myocytes from different regions of the rainbow trout ventricle at 12°C. (**A-C**) Inward rectifier K^+ current (I_{K1}). (**A**) Voltage protocol and representative I_{K1} tracings at different membrane potentials. (**B**) Representative I_{K1} tracings showing the voltage-dependence of I_{K1}. Peak densities of inward (I.C.) and outward (O.C) I_{K1} are shown in the inset. (**C**) Transcripts of Kir2 inward rectifier K^+ channel genes. The results are means (±SEM) of 11-13 myocytes from 4 fishes for I_{K1} recordings and from 6 fish for transcript expression. (**D-F**) Delayed rectifier K^+ current (I_{Kr}). (**D**) Voltage protocol and representative I_{Kr} tracings at different membrane potentials. The arrow indicates the point of measurement (the maximum tail current amplitude). (**E**) Current-voltage relationships of I_{Kr} from different regions of trout ventricle. The inset shows the peak tail current densities and their statistical comparison at +80 mV. (**F**) Transcript expression of KCNH2bb and KCNH6a channels. The results are means (±SEM) of 15-20 myocytes from 5 fishes for I_{Kr} recordings and from 6 fish for transcript expression. An asterisk (*) indicates statistically significant differences ($p < 0.05$; one-way ANOVA) between means.

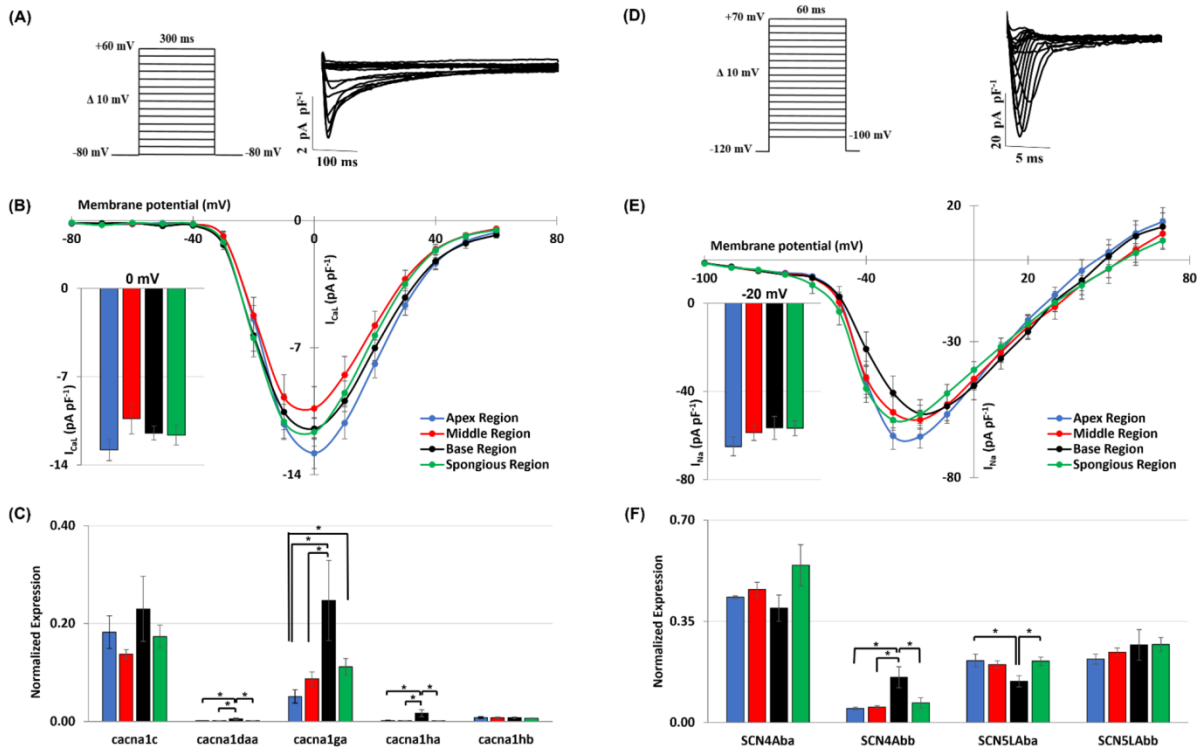

Fig. 3. Ca^{2+} and Na^{+} currents in myocytes from different regions of the rainbow trout ventricle at 12°C. (**A-C**) Ca^{2+} current (I_{Ca}). (**A**) Voltage protocol and representative I_{Ca} tracings at different membrane potentials. (**B**) Mean current-voltage relationships of I_{Ca} in the 4 different regions of the trout ventricle. The inset shows the peak current densities at 0 mV and their statistical comparison. (**C**) Expression of Ca^{2+} channel transcripts in the 4 ventricular regions. The results are means (±SEM) of 13-17 myocytes from 4 fishes for I_{Ca} recordings and from 6 fish for transcript expression. (**D-F**) Na^{2+} current (I_{Na}). (**D**) Voltage protocol and representative I_{Na} tracings at different membrane potentials. (**E**) Mean current-voltage relationships of I_{Na} in the 4 different regions of the trout ventricle. The inset shows the peak I_{Na} densities at −20 mV and their statistical comparison. (**F**) Expression of Na^{2+} channel transcripts in the 4 ventricular regions. The results are means (±SEM) of 10-12 myocytes from 3 fishes for I_{Na} recordings and from 6 fish for transcript expression. An asterisk (*) indicates statistically significant differences ($p < 0.05$; one-way ANOVA) between means.

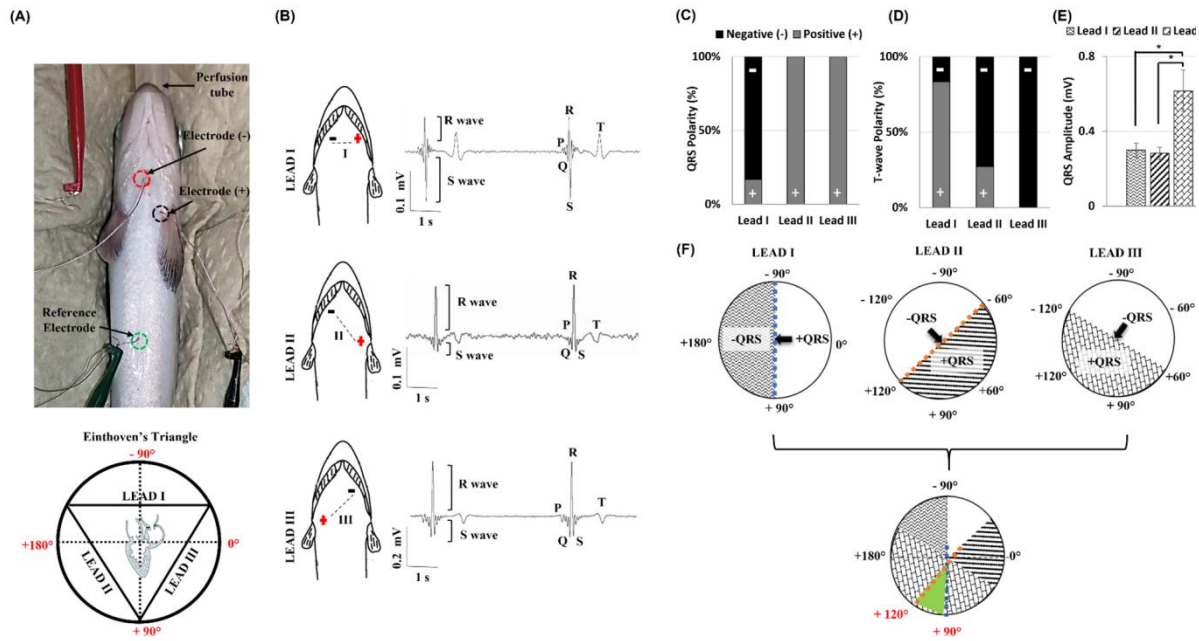

Fig. 4. Determination of the heart axis (the main direction of ventricular depolarization) in rainbow trout by *in vivo* ECG recordings at 16℃. (**A**) ***top:*** ECG recording set-up in anesthetized rainbow trout lying on a damped sponge and orally perfused for aeration. Bipolar electrodes are inserted at their locations for Lead II of the Einthoven's triangle (red and black circles) and the reference electrode inserted near the anus (green circle). ***bottom:*** A diagram shows the directions of the 3 pairs of electrodes used to construct 3 leads (I-III) for the Einthoven's triangle (*see methods*). (**B**) Representative ECG recordings from the 3 leads. P, atrial depolarization; QRS complex, ventricular depolarization; T, ventricular repolarization; R wave, the positive deflection of QRS complex away from the isoelectric baseline; S wave, the negative deflection of QRS complex away from the isoelectric baseline. (**C**) Polarity percentage of QRS complex in the 3 leads. (**D**) Polarity percentage of T-wave in the 3 leads (**E**) Amplitude of the QRS complex in the 3 ECG leads. (**F**) The main direction of depolarization in the 3 ECG leads, where the overlapping between them resulted in the trout heart axis between +90°- +120° (green sector). Results are from 11 fishes. An asterisk (*) indicates statistically significant differences ($p < 0.05$; one-way ANOVA) between means.

Table 1. Composition of internal (pipette) saline solutions in current clamp and voltage clamp experiments in mmol L^{-1}.

	Action potentials	Potassium currents (I_{Kr}, I_{K1})	Sodium current (I_{Na})	Calcium current (I_{CaL})
NaCl			5	
KCl	140	140		
CsCl			130	130
$MgCl_2$	1	1	1	1
TEACl*				15
Oxaloacetate				5
MgATP	4	4	5	5
EGTA	5	5	5	5
HEPES	10	10	5	10
cAMP**				0.02
pH	7.2 (KOH)	7.2 (KOH)	7.2 (CsOH)	7.2 (CsOH)

(Badr et al., 2017), (Badr et al., 2018); * tetraethyl ammonium chloride; ** cyclic adenosine monophosphate

Table 2 Composition of the external saline solution in current clamp and voltage clamp experiments in mmol L^{-1}

	Action potentials	I_{Kr} potassium current	I_{K1} potassium current	Sodium current (I_{Na})	L-type Ca current (I_{CaL})
NaCl	150	150	150	20	150
KCl	3	3	3		
CsCl				120	5.4
$MgCl_2$				1	1.2
$MgSO_4$	1.2	1.5	1.5		
NaH_2PO_4	1.2	0.4	0.4		
$CaCl_2$	1.8	2.0	2.0	0.5	1.8
Glucose	10	10	10	10	10
HEPES	10	10	10	10	10
***TTX**		0.0005	0.0005		0.0005
Nifedipine		0.01	0.01	0.01	
$BaCl_2$		0.2			
E-4031			0.004		
pH (20°C)	7.6 (NaOH)	7.6 (KOH)	7.6 (KOH)	7.6 (CsOH)	7.6 (CsOH)

(Badr et al., 2017), (Badr et al., 2018); *tetrodotoxin

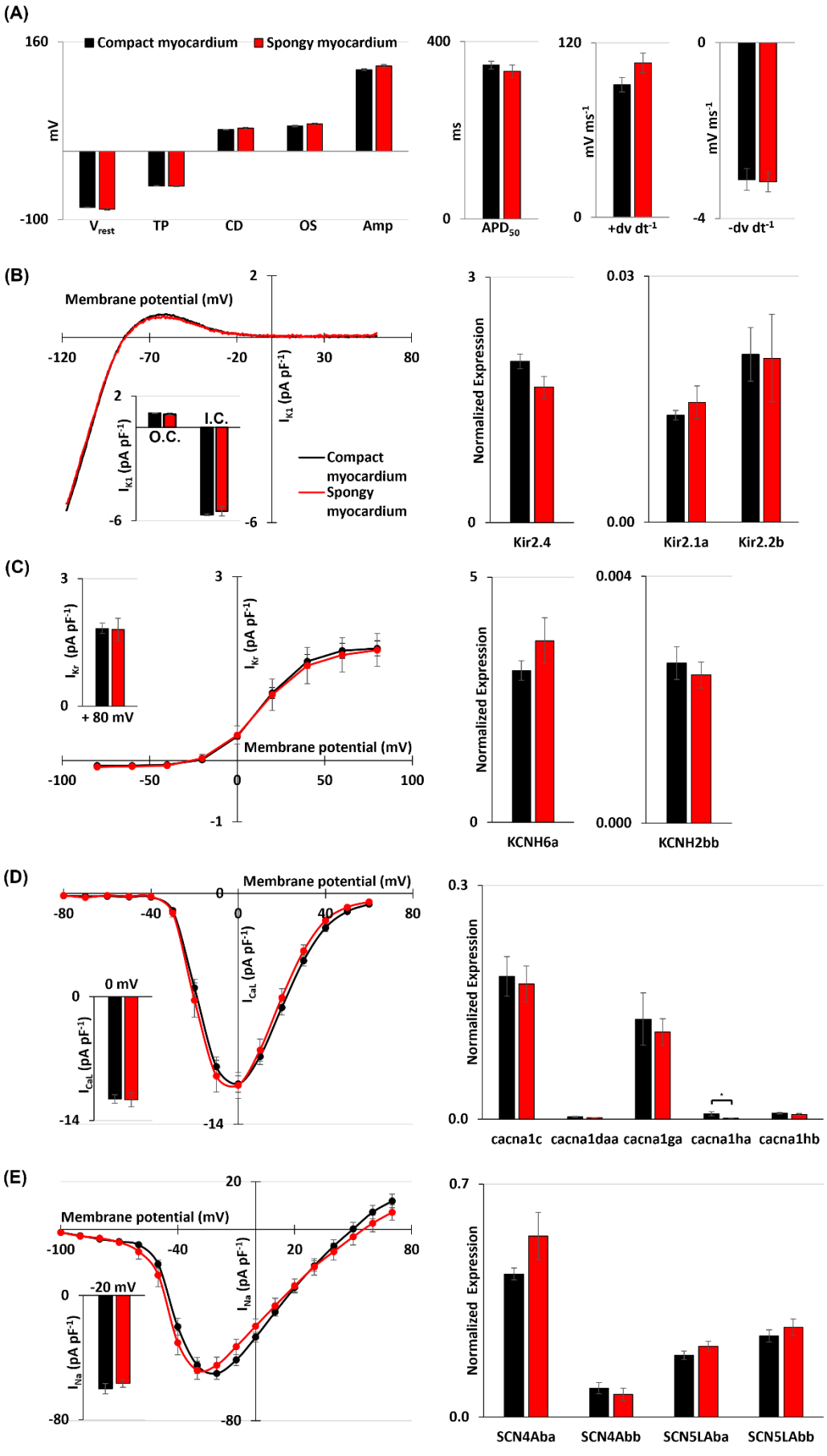
(A)
Compact myocardium
Spongy myocardium
mV
160
-100
V_{rest}
TP
CD
OS
Amp
ms
400
0
APD_{50}
mV ms^{-1}
120
0
+dv dt^{-1}
0
-4
-dv dt^{-1}
(B)
Membrane potential (mV)
-120
-70
-20
30
80
2
-6
I_{K1} (pA pF^{-1})
O.C.
I.C.
Compact myocardium
Spongy myocardium
Normalized Expression
3
0
Kir2.4
0.03
0.00
Kir2.1a
Kir2.2b
(C)
I_{Kr} (pA pF^{-1})
+ 80 mV
Membrane potential (mV)
-100
-50
50
100
-1
5
KCNH6a
0.004
0.000
KCNH2bb
(D)
Membrane potential (mV)
-80
-40
40
80
0 mV
I_{CaL} (pA pF^{-1})
-14
0.3
0.0
cacna1c
cacna1daa
cacna1ga
cacna1ha
cacna1hb
(E)
Membrane potential (mV)
-100
-40
20
80
-20 mV
I_{Na} (pA pF^{-1})
-80
0.7
SCN4Aba
SCN4Abb
SCN5LAba
SCN5LAbb

Fig. S1. Comparison of action potential (AP) parameters, sarcolemmal ion currents, and ion channel expression between compact (pooled data from apex, middle and basal regions) and spongy myocardium of rainbow trout ventricle. (**A**) Ventricular APs parameters: resting membrane potential (V_{rest}), threshold potential for AP initiation (TP), critical depolarization (CD), AP overshoot (OS), AP amplitude (Amp), AP duration at 50% level of repolarization (APD_{50}), maximum rate of depolarization (+dV dt^{-1}), and repolarization (-dV dt^{-1}). (**B-C**) Inward (I_{K1}) and delayed rectifier (I_{Kr}) K^+ currents (left), and transcripts of Kir2 (I_{K1}), KCNH2bb and KCNH6a (I_{Kr}) channels (right). The insets show peak densities of inward (I.C.) and outward (O.C) of I_{K1} (**B**), and peak tail current densities of I_{Kr} at +80 mV (**C**). (**D-E**) Ca^{2+} (I_{CaL}) and Na^+ (I_{Na}) currents (left), and transcripts of Ca^{2+} and Na^+ channels (right). The insets show the peak current densities of I_{CaL} at 0 mV (**D**), and I_{Na} at -20 mV (**E**). An asterisk (*) indicates statistically significant differences ($p < 0.05$; *t*-test) between mean values.

Table S1.

Click here to download Table S1